



HAL
open science

Binary and Ternary Core–Shell Crystals of Polynuclear Coordination Clusters via Epitaxial Growth

Le Shi, Jędrzej Kobylarczyk, Kamil Kwiatkowski, Barbara Sieklucka, Sylvie Ferlay, Robert Podgajny

► **To cite this version:**

Le Shi, Jędrzej Kobylarczyk, Kamil Kwiatkowski, Barbara Sieklucka, Sylvie Ferlay, et al.. Binary and Ternary Core–Shell Crystals of Polynuclear Coordination Clusters via Epitaxial Growth. *Crystal Growth & Design*, 2022, 22 (5), pp.3413-3420. 10.1021/acs.cgd.2c00216 . hal-03780255

HAL Id: hal-03780255

<https://cnrs.hal.science/hal-03780255>

Submitted on 20 Sep 2022

HAL is a multi-disciplinary open access archive for the deposit and dissemination of scientific research documents, whether they are published or not. The documents may come from teaching and research institutions in France or abroad, or from public or private research centers.

L'archive ouverte pluridisciplinaire **HAL**, est destinée au dépôt et à la diffusion de documents scientifiques de niveau recherche, publiés ou non, émanant des établissements d'enseignement et de recherche français ou étrangers, des laboratoires publics ou privés.

Binary and Ternary Core-Shell Crystals of Polynuclear Coordination Clusters via Epitaxial Growth

Le Shi,^a Jędrzej Kobylarczyk,^{a,b} Kamil Kwiatkowski,^a Barbara Sieklucka,^a Sylvie Ferlay^c and Robert Podgajny^{,a}*

AUTHOR INFORMATION

Corresponding Author

Robert Podgajny - *^aFaculty of Chemistry, Jagiellonian University, Gronostajowa 2, 30-387 Krakow, Poland, e-mail: robert.podgajny@uj.edu.pl.*

Authors

Le Shi - *^aFaculty of Chemistry, Jagiellonian University, Gronostajowa 2, 30-387 Krakow, Poland, e-mail: leshiyun1994@163.com.*

Jędrzej Kobylarczyk - *^aFaculty of Chemistry, Jagiellonian University, Gronostajowa 2, 30-387 Krakow, Poland; ^bInstitute of Nuclear Physics PAN, Radzikowskiego 152, 31-342 Kraków, Poland; e-mail: jedrzej.kobylarczyk@ifj.edu.pl; jedrzej.kobylarczyk@uj.edu.pl*

Kamil Kwiatkowski - *^aFaculty of Chemistry, Jagiellonian University, Gronostajowa 2, 30-387 Krakow, Poland; email: kwiatkowski.kamil484@gmail.com.*

Barbara Sieklucka - *^cFaculty of Chemistry, Jagiellonian University, Gronostajowa 2, 30-387 Krakow, Poland; e-mail: barbara.sieklucka@uj.edu.pl*

Sylvie Ferlay - *^cUniversity of Strasbourg, CNRS, CMC UMR 7140, F-67000 Strasbourg, France; e-mail: ferlay@unistra.fr*

ABSTRACT

For the first time, an abundant series of 12 colorful binary and ternary mm sized core-shell composite crystals, representative of hierarchical crystalline species, was designed and prepared from functional magnetic polynuclear clusters phases, using the epitaxial growth method. The building is based on isomorphous (space group $C2/c$) crystalline phases composed of 15-nuclear clusters $\{M_9[W^V(CN)_8](MeOH)_{24}\}$ (M_9W_6) (M , color = Mn^{II} , pale brown; Fe^{II} , green; Co^{II} , red; Ni^{II} yellow; Fe/Co 2:1 mixture, dark brown) of six-capped-body-centered-cube topology, revealing appealing magnetic properties such as high-spin in the ground state, slow magnetic relaxation and structural-spin phase transitions. A series of 11 binary core-shell composites and 1 ternary composite has been reproducibly synthesized, and carefully characterized from a structural and composition point of view. Phase composition accordance and size of interface of *ca.* 10 μm were assessed using microscopic observations, SC-XRD, and SEM-EDS. SQUID measurements reveals an active spin transition $Fe_6Co_3W_6$ seed compound enveloped within the paramagnetic Mn_9W_6 crystalline shell, providing a rare example of mm-sized hierarchical crystalline architecture $Fe_6Co_3W_6@Mn_9W_6$ with switchable function.

INTRODUCTION

Molecular crystals, due to their periodic intrinsic organization and their transparency, may exhibit tunable physical properties and functions and they continue to attract attention as promising platforms for application in optoelectronic,¹ energy conversion,² molecular switches^{3,4} or chemical sensors.⁵ Molecular crystals can be built from metal centers, ligands or guest molecules, periodically embedded at dedicated crystallographic sites in different parts of the crystalline solid. Of particular interest in this field, and due to the enhancement of some properties, is the obtention of molecular crystals with hierarchical structures, which

implies a particular processing of the crystals, being divided in different organized “zones”.⁶

Among the hierarchical crystalline architectures, the core-shell crystals draw notable interest. The nanometric examples of core-shell nanoparticles (NPs) based on magnetic cyanido-bridged networks were reported, showing a variety of possible shapes and sizes, ranging from 50 nm to 150 nm. Owing to hierarchical character of the construction, and thanks to the isostructural character of the underlying crystalline phases, some of them exhibit magnetic properties slightly different from those reported for the nanoparticles of the pure phases;^{7,8} some of them also present photomagnetic behavior.^{9,10} At the microscopic level, core-shell molecular crystals¹¹⁻¹⁴ or welded crystals¹⁵⁻¹⁷ represent nice examples of μm or mm size hierarchical structures, obtained through the epitaxial growth of one phase on the external surface (shell) of the another isostructural phase (seed crystal or core), as already reported. This is a biphasic growth process, occurring at RT, arising at the solid/liquid interface which may occur when one or more molecular components can be interchanged between the core crystal and the shell crystal, at the dedicated sites of crystal structure. Weak intermolecular interactions such as hydrogen and halogen bonds, π - π interaction, anion/cation- π interaction, and labile coordination bonds between molecular components facilitate the controlled arrangement in such self-assembled hierarchical architectures. Nevertheless, numerous reports involving extended coordination hierarchical crystalline architectures like metal-organic frameworks (MOFs)¹⁸⁻²⁵ or ionic salts²⁶ with stronger inter-component binding were also described, exhibiting gas selectivity and storage, heterogeneous catalysis, multicolor luminescence, or conductivity. However, the construction of μm or mm sized core-shell crystalline composites based on molecular magnetic and switchable materials remains still unexplored, and may be achieved through incorporation of polynuclear coordination clusters, for example.

As an appropriate basis for a new unique core-shell crystals family, we selected the colorful series of crystalline phases composed of 15-nuclear cyanido-bridged isolated

clusters $\{M_9[W^V(CN)_8]_6(MeOH)_{24}\}$ (M_9W_6) ($M = Mn^{II}, Fe^{II}, Co^{II}, Ni^{II}$) (Figure 1a).²⁷⁻³² All clusters display a structure based on a six-capped-body-centred-cube, with the central $[M(\mu-NC)_6]$ moiety surrounded by six $[W(\mu-CN)_5(CN)_3]^{3-}$ moieties located in the corners of the super-octahedron, and further, by eight $[M(\mu-NC)_3(MeOH)_3]$ moieties located in the corners of the concentric super-cube (Figure 1b). The related phases exhibit similar crystal morphology and strict isomorphism within the monoclinic space group $C2/c$, yet diverse colors and a variety of magnetic properties such as high spin in the ground state, slow magnetic relaxation, charge transfer and spin transition, depending on the embedded metal ions. Taking advantage of the isomorphous and almost isometric nature of all reported crystal lattices, recently we have also demonstrated a growth of multicomponent $M_6M''_3W_6$ systems - *trimetallic* molecular solid solutions - simply by adjusting the trimetallic compositions during the crystal formation. The heterotrimetallic $Fe_xCo_{9-x}W_6$ clusters exhibited simultaneous Electron Transfer (ET) and Charge Transfer Induced Spin Transition (CTIST) through the $Co-N\equiv C-W$ and $Fe-N\equiv C-W$ linkages,^{33,34} the $Fe_9Re_{6-x}W_6$ analogues revealed competition between Fe^{II} Spin Crossover (SCO) centres and ET through $Fe-N\equiv C-W$ linkages,³⁵ whereas $Ni_xCo_{9-x}W_6$ and $Mn_xCo_{9-x}W_6$ derivatives systematically exhibited tuneable spin in the ground state and slow magnetic relaxation.³⁶ The above features provide prerequisites towards further exploration of multicomponent molecular approach, of the related potentially functional crystalline composites *via* epitaxial growth.

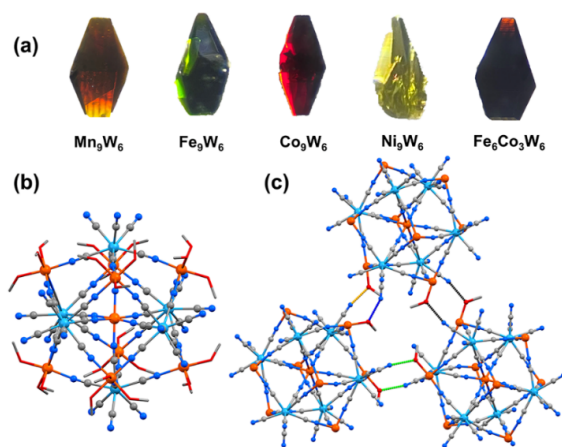


Figure 1. (a) Pictures of single crystals of the bimetallic $\mathbf{M}_9\mathbf{W}_6$ ($M = \text{Mn, Fe, Co, Ni}$) and trimetallic $\mathbf{Fe}_6\mathbf{Co}_3\mathbf{W}_6$ crystals of pentadecanuclear clusters exhibiting visually distinguishable colors. (b) The molecular structure of $\mathbf{M}_9\mathbf{W}_6$ ($M = \text{Mn, Fe, Co, Ni}$) and trimetallic $\mathbf{Fe}_6\mathbf{Co}_3\mathbf{W}_6$ pentadecanuclear clusters obtained from SC XRD data.²⁷⁻³⁰ (c) The direct hydrogen-bonded interactions between clusters. Color code: 3d metal ion – orange; W – cyan; C – grey, N – blue; O – red. H atoms and crystallization molecules of methanol are omitted for clarity.

The key property towards successful construction of the above targeted core-shell crystals is the nature and quality of the intermolecular interactions between clusters, here realized *via* the direct hydrogen bonds involving coordinated methanol molecules and terminal cyanido ligands (Figure 1c). Hydrogen bond, by its nature, provides suitable span of D...A distances and D-H...A angles that should allow to compensate for slight mismatch of unit cell parameters between the isostructural core and shell crystals, and support formation of the interface.¹¹⁻¹⁴ Furthermore, since these crystals exhibit colors discernible by naked eye, pale brown for $\mathbf{Mn}_9\mathbf{W}_6$, green for $\mathbf{Fe}_9\mathbf{W}_6$, red for $\mathbf{Co}_9\mathbf{W}_6$, yellow for $\mathbf{Ni}_9\mathbf{W}_6$ and dark brown for $\mathbf{Fe}_6\mathbf{Co}_3\mathbf{W}_6$ solid solution (Figure 1a), one can easily monitor the epitaxial growth process by color contrast on the surface of the seed crystals.

In this work, we present the synthesis and complete structural and composition characterization of molecular core-shell composites belonging to this family, and for one of them, offering a switchable core, we assess the magnetic behavior.

EXPERIMENTAL SECTION

Materials

All chemicals and materials were purchased from commercial sources (Sigma-Aldrich and TCI), and used without further purification. Octacyanidotungstate salts, $\text{K}_4[\text{W}(\text{CN})_8]\cdot 2\text{H}_2\text{O}$ and

TBA₃[W(CN)₈] (TBA = tetrabutylammonium cation) were synthesized according to the published procedures.^{37,38}

Synthesis of mono-phase crystals

Suitable size crystals of **M₃W₆** (M = Fe, Co, Ni, Mn) and **Fe₆Co₃W₆** were prepared following the already reported with a slightly modified method.^{27-30,33} In a typical experiment, the methanolic solution (2 ml) of TBA₃[W(CN)₈] (37.5 mg, 0.033 mmol) was quickly mixed with the methanolic solution (3 ml) of 0.05 mmol 3d metal ions (Fe, Co, Ni, Mn, Fe:Co = 2:1 for **Fe₆Co₃W₆**) in a vial. For the high soluble **Ni₃W₆** and **Mn₃W₆**, the ethyl ether (2 ml) was slowly added to the solution. The resulting solution was tightly closed and left for crystallization in the dark. After several days, a large amount of block crystals of the relevant color appeared in the bottom.

Synthesis of core-shell crystalline composites

Core-shell crystalline composites **M₃W₆@M'₃W₆** were obtained by immersing the seed crystals of **M₃W₆** into a methanolic solution containing TBA₃[(W(CN)₈)₃] and the corresponding M'Cl₂ salts (M' = Fe, Co, Ni, Mn). The detailed amounts of substrates and the reaction time are listed in **Table 1**. The growth process was monitored with an optical microscope. Core-shell crystals formations was completed in a few hours to a few days period, depending on the nature of the used 3d metal ion M' salts.

General physical techniques

The growth and identity of our core-shell crystals were assessed by optical microscopic observation, SC-XRD, and SEM-EDS techniques, providing the well suited protocol used for crystalline composites. SQUID magnetometry was applied to verify the behavior of the selected composite of interest.

Single crystal X-ray diffraction data for all crystals were collected using Bruker D8 Quest Eco diffractometer equipped with Photo50 CMOS detector, Mo K α ($\lambda = 0.71073$ Å) radiation source with a graphite monochromator and Bruker Cryoflex II cooling system. Crystals for measurement were taken from mother solution and mounted on MiteGen Micro loops using NVH immersion oil or apiezon grease. Measurements were performed at 100 K for all crystals. Data

Table 1. Detailed concentrations and volumes of the *shell* solutions and the related duration times of the growth of the shell phase on the core phase.

Composites	Concentration of TBA ₃ [W(CN) ₈] / mol L ⁻¹	Concentration of M'Cl ₂ salts / mol L ⁻¹	Volume of MeOH / mL	Time / h
Co₉W₆@Ni₉W₆	0.022	0.033	3	168
Fe₉W₆@Ni₉W₆	0.022	0.033	3	168
Ni₉W₆@Co₉W₆	0.033	0.05	2	2
Fe₉W₆@Co₉W₆	0.0033	0.005	10	48
Co₉W₆@Fe₉W₆	0.0033	0.005	10	48
Co₉W₆@Mn₉W₆	0.0055	0.0083	6	2
Fe₉W₆@Mn₉W₆	0.0055	0.0083	6	2
Fe₆Co₃W₆@Ni₉W₆	0.022	0.033	3	168
Fe₆Co₃W₆@Fe₉W₆	0.0033	0.005	10	48
Fe₆Co₃W₆@Co₉W₆	0.0033	0.005	10	48
Fe₆Co₃W₆@Mn₉W₆	0.0055	0.0083	6	48
Fe₉W₆@Co₉W₆@Ni₉W₆	0.022	0.033	3	168

reduction and cell parameter refinement were performed using Apex software with included SAINT³⁹ and SADABS⁴⁰ programs. Intensities of reflections for the sample absorption were corrected using multi-scan method. The structural figures were prepared using latest Mercury software.⁴¹

The SEM-EDS measurements were performed using JEOL-5410 SEM microscope equipped with EDS NORAN Voyager 3100 add-on. The selected five composites were taken from mother solution and dispersed on NVH immersion oil. The samples have been obtained by carefully cutting composites perpendicular to the longest axis of the crystal. Cutting samples are dried in air and transferred to the SEM grids (carbon film on a holey carbon support film).

Magnetic measurements were investigated using Quantum Design MPMS 3 SQUID magnetometer. For the measurements $\text{Fe}_6\text{Co}_3\text{W}_6$ crystals and $\text{Fe}_6\text{Co}_3\text{W}_6@\text{Mn}_9\text{W}_6$ crystalline composites were separately sealed in glass tubes with a small amount of mother solution under vacuum. The dc magnetic susceptibilities were measured in the 175 – 295 K temperature range with an applied field of 1000 Oe in a sweep mode with the scan rate of 1 K min⁻¹. The magnetic data were corrected for diamagnetic contribution of the glass tube and sample by empirical and Pascal's constants.⁴² The integrity of the $\text{Fe}_6\text{Co}_3\text{W}_6@\text{Mn}_9\text{W}_6$ core-shell crystals after a thermal cycle was assessed by the optical microscopy observation (*for details see SI section*).

RESULTS AND DISCUSSION

Synthesis and crystal growth

Typical preparation procedure for the formation of composite core-shell crystals is based on the immersion of the seed crystals (M_9W_6 or $\text{M}_6\text{M}'_3\text{W}_6$) in a methanolic solution containing a stoichiometric amount of $\text{TBA}_3[\text{W}^{\text{V}}(\text{CN})_8]$ and $\text{M}^{\text{III}}\text{Cl}_2$ salts (see Experimental part). As a result, a series of eleven binary core-shell crystalline objects combining different cores, Co_9W_6 , Fe_9W_6 , Ni_9W_6 , $\text{Fe}_6\text{Co}_3\text{W}_6$, and shells, Ni_9W_6 , Fe_9W_6 , Co_9W_6 , Mn_9W_6 ($\text{M}'_9\text{W}_6$) were reproducibly obtained (Table 1), hereafter denoted by $\text{M}_9\text{W}_6@\text{M}'_9\text{W}_6$ (or $\text{M}_6\text{M}'_3\text{W}_6@\text{M}'_9\text{W}_6$) ($\text{M}, \text{M}' = \text{Fe}, \text{Co}, \text{Ni}, \text{Mn}; \text{M}'' = \text{Co}$), denoted as composites core@shell. Their pictures are presented in Figure 2, showing a satisfying color contrast between the

core and the shell. Moreover, the ternary crystalline composite, denoted as $\text{Fe}_9\text{W}_6@Co_9\text{W}_6@Ni_9\text{W}_6$ (Figure 2, bottom right) was also successfully obtained by immersing as-synthesized $\text{Fe}_9\text{W}_6@Co_9\text{W}_6$ crystals, behaving as a “core-crystal” in a methanolic solution containing the components for the formation of the shell $Ni_9\text{W}_6$.

The growth rate of the shell notably depends on the object composition. Some general trends were observed. (i) The composites involving Fe_9W_6 , $Co_9\text{W}_6$, or $Mn_9\text{W}_6$ as

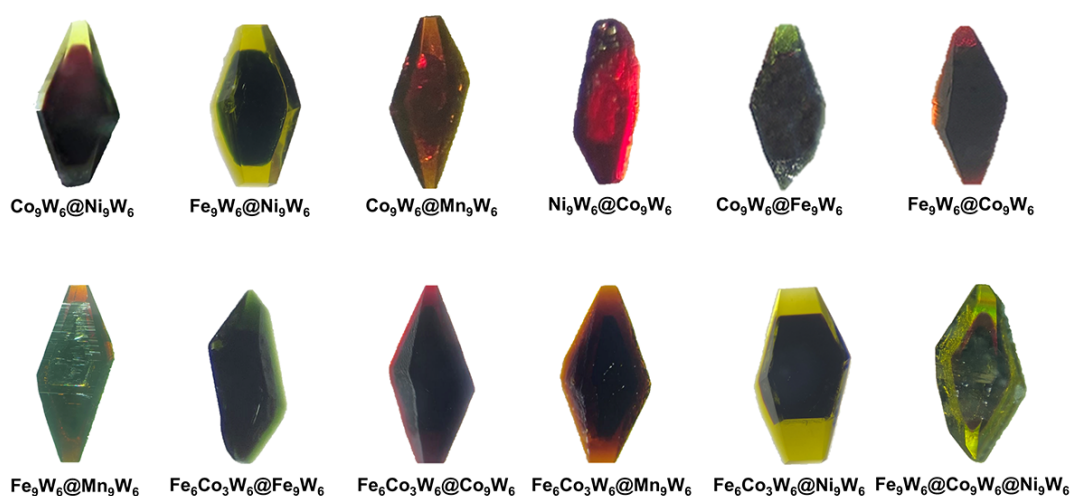


Figure 2. Photographs of a series of core-shell crystals $M_9W_6@M'_9W_6$ or $Fe_6Co_3W_6@M'_9W_6$. The last image in the second row shows the ternary composite $Fe_9W_6@Co_9W_6@Ni_9W_6$.

a shell can be grown within several hours, whereas those with Ni_9W_6 shell requires *ca.* 1 week. This is consistent with the growth rate of the pure bimetallic phases M_9W_6 . (ii) The solubility of the bimetallic (or trimetallic) species (M_9W_6 or $M_6M''_3W_6$) is dependent on the nature of the involved metals. Due to high solubility in the core-shell growth conditions, Ni_9W_6 and Mn_9W_6 can hardly be considered as seed crystal (see experimental part). When used as shell, Ni_9W_6 require significantly higher concentrations to accomplish the composite formation. Anyway, Mn_9W_6 forms shell relatively quickly, which might be correlated with the largest cell volume of the series. (iii) Interestingly, in the case of composites $Co_9W_6@Ni_9W_6$, $Fe_9W_6@Ni_9W_6$, and $Fe_6Co_3W_6@Ni_9W_6$ (Figure 3) the growth

rate is faster on the top and on bottom surface or edge perpendicular to the longest composite axis, which indicates the preferential growth directions for these species. This will be further detailed in the X-Rays studies section.

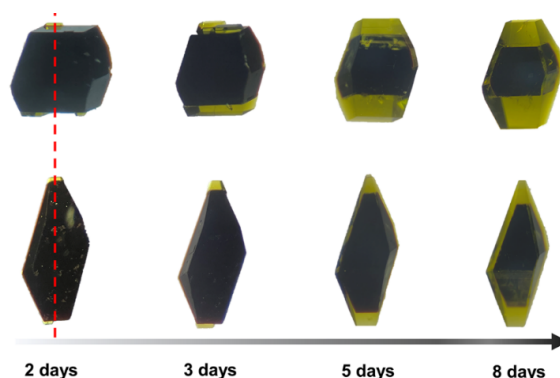


Figure 3. The sequential growth of the selected $M_9W_6@M'_9W_6$ core-shell crystals (taking $Fe_6Co_3W_6@Ni_9W_6$ as an example): (i) tiny crystals on the top or bottom surface or edge of core crystals perpendicular to the longest crystal axis appear within 2 days; (ii) after 3 days, the shell gradually fills the uneven area on the top or bottom, the tiny crystals start to appear on the side surface; (iii) after 5 to 8 days, very well core-shell crystals are formed. The dashed red line indicates the longest axis (top) or the C_4 symmetry axis (bottom) of crystal, depend on the crystal morphology.

X-ray studies

The composite crystals were first characterized using XRD on single crystals. The identity of the shell lattice of the formed composites $Co_9W_6@Ni_9W_6$, $Fe_9W_6@Co_9W_6$, $Co_9W_6@Fe_9W_6$, $Fe_6Co_3W_6@Fe_9W_6$, $Fe_6Co_3W_6@Co_9W_6$ and $Fe_6Co_3W_6@Mn_9W_6$ was confirmed by single-crystal XRD measurement of cell parameters on various composite fragments at 100 K, by focusing the X-ray beam on desired domains (Figure 4 and Figures S1-S5). The characterization is performed individually, on each composite behaving as a single crystal. As shown in SI, the cell parameters of the shell fragments are very close to the ones of mono-phase crystals (Tables S1-S7). Taking the $Co_9W_6@Ni_9W_6$ crystalline

composite as an example, the cell parameters of the shell fragment was found to be $a = 28.4740(12) \text{ \AA}$, $b = 19.1838(8) \text{ \AA}$, $c = 32.3271(11) \text{ \AA}$, $\beta = 113.39(1) \text{ deg.}$ and $V = 16207.1(11) \text{ \AA}^3$, almost identical to those observed for Ni_9W_6 crystals.²⁸

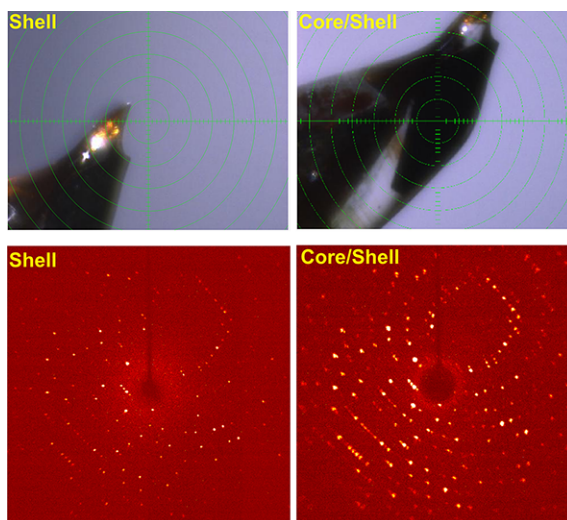


Figure 4. Single-crystal XRD measurements for the core-shell crystalline composite. X-ray beam on the shell part and on the core/shell part (right) of crystal (top). The representative diffraction frames of $\text{Co}_9\text{W}_6@Fe_9\text{W}_6$ evidencing the epitaxial growth character within the composite. (bottom).

During the epitaxial growth process, the crystallographic axes are maintained, as shown by the shape of the shell growing around the seed crystal, and also as attested by the crystallographic frames illustrating the accordance of the spots patterns for the composites $\text{Co}_9\text{W}_6@Ni_9\text{W}_6$, $Fe_9\text{W}_6@Co_9\text{W}_6$, $Co_9\text{W}_6@Fe_9\text{W}_6$, $Fe_6Co_3W_6@Fe_9\text{W}_6$, $Fe_6Co_3W_6@Co_9\text{W}_6$ and $Fe_6Co_3W_6@Mn_9\text{W}_6$ at the central zone (representing core and shell diffraction), and at the peripheral zone (representing only the shell diffraction). All the composites behave as single crystals.

The Faces Indexing crystal experiments (Figure 5) confirmed that the (001) face constitutes a plane with “smoother” H-bonding surface compared to other faces. Such arrangement probably directs the lattice spacing of the (001) layer of the core crystal, and

facilitates the directional core growth or accommodates the built-up of an incoming epitaxial layer in a more favorable direction perpendicular to the (001) face.⁴³ This is in accordance with the nature of the axis of preferential growth that has been evidenced during the growth process (see Figure 3).

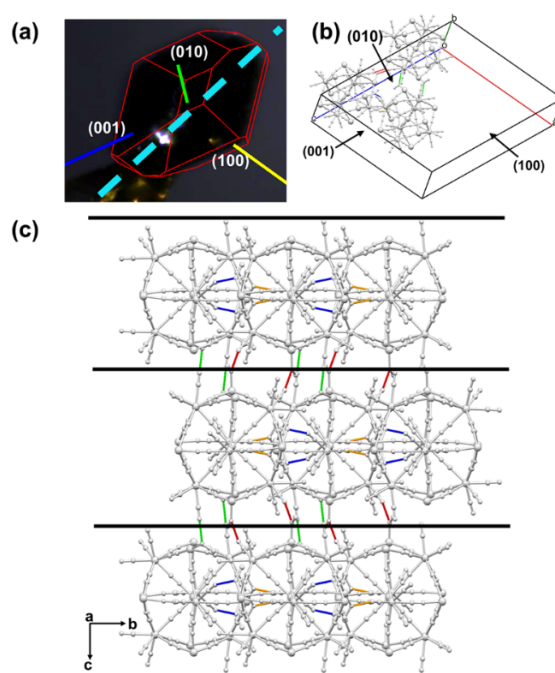


Figure 5. Face indexing image (a) and the direct hydrogen-bonded directions in the related packing diagram (b) for the $\text{Fe}_6\text{Co}_3\text{W}_6$ crystal. The solid lines in represent the directions perpendicular to the three major faces, and the dashed line shows the longest axis of the crystal. (c) Side-views along of the (001) plane (converging with the “smooth” surface of cluster layer; dark solid line) in the direction perpendicular to the (100) plane and (010) plane.

SEM-EDS characterization

SEM-EDS technique was used to describe the compositional changes along the cross-section of the selected composites, that may be divided in “zones”, as observed in hierarchical crystalline species, obtained through the perpendicular cut in respect to its longest axis (Figure 6). The point analysis (average atomic ratio) for $\text{Co}_9\text{W}_6@Fe_9W_6$,

Fe₉W₆@Co₉W₆, **Fe₆Co₃W₆@Mn₉W₆**, **Fe₆Co₃W₆@Co₉W₆** and **Fe₆Co₃W₆@Fe₉W₆** reliably reproduced the relative contents of the metals located in the shell and core respectively (Tables S8-S17). However, the observed data also show some deviations in both shell and core parts, which could be explained in terms of core surface dissolution and migration of the metal ions during the formation of the composite, at the solid/liquid interface, in agreement with previous observations for the core-shell crystals based on the hydrogen bonded phases.⁴⁴

The Line Scan Profiles (LSP) for **Co₉W₆@Fe₉W₆** and **Fe₉W₆@Co₉W₆** illustrate the variations of the count rate of Co-K and Fe-K emission perpendicular to the interface (Figure 6b, c and Figure S6, SI). For the **Co₉W₆@Fe₉W₆** composite, the percentage of Co-K typically decreases from 87% to 15% when going through the interface, while the percentage of Fe-K increases from 13% to 85%. This matches well with the domination of separated **Co₉W₆** and **Fe₉W₆** phase at the appropriate areas. The complementary observations were also done for **Fe₉W₆@Co₉W₆**. In the middle position in the Fig. 6b and Fig. S8b, SI, the sharp changes in the percentage of Fe-K and Co-K corresponds to the solid solution interface area, which presents a thickness of *ca.* 10 μm for both **Co₉W₆@Fe₉W₆** and **Fe₉W₆@Co₉W₆** composites.

Magnetic properties

The synergies between core and shell architectures distributed in independent domains could affect their functionalities, for example based on modified magnetic properties, as already observed for molecular magnetic NPs.⁷⁻¹⁰ Theoretical and experimental studies have suggested

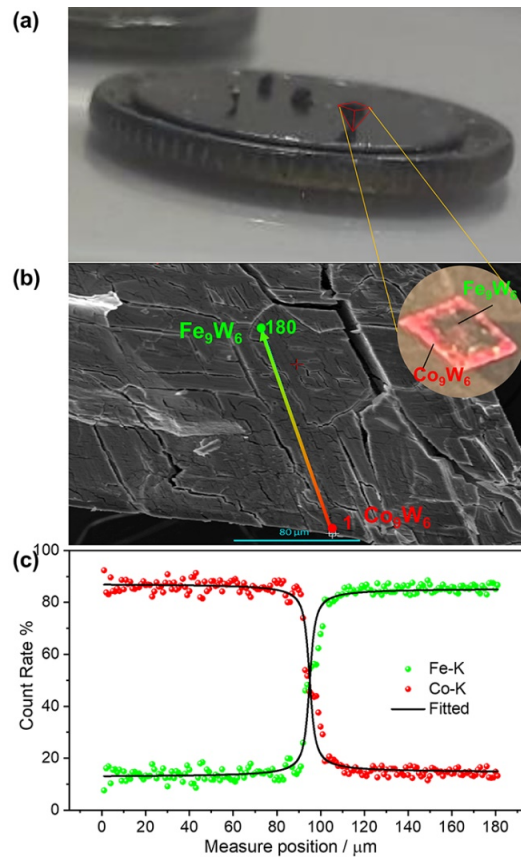


Figure 6. (a) Representative photographs of the composites prepared for SEM-EDS measurements; (b) The SEM image (500x zoom applied) of the cross-section fragment obtained by cutting the $\text{Fe}_9\text{W}_6@ \text{Co}_9\text{W}_6$ composite perpendicular to the longest axis of the crystal. The red-to-green line of the length of $180 \mu\text{m}$ indicate the LSP crossing the interface area. Inset: the optical image of the cross-section. (c) The relevant illustration of the change in Co (red circles) and Fe (green circles) contents during the SEM-EDS scan. The scan step is $1 \mu\text{m}$. The sigmoidal fits indicate the longitudinal size of the interface (for other SEM-EDS data see SI section).

that the interface on the external surface of the material can affect the magnetic behavior of the material through perturbation of surface energy, which might be particularly crucial in the case of materials exhibiting spin transition phenomenon.⁴⁵⁻⁴⁹ Along this line, we intend to explore the magnetic properties of composites exhibiting thermal switchable behavior, as observed in the

Fe₆W₆ and **Fe₆Co₃W₆** phases.^{30,33} They undergo a reversible simultaneous ET between W^{IV}-C≡N-^{HS}Fe^{III} or W^V-C≡N-^{HS}Fe^{II} states or/and combined ET/CTIST between the W^{IV}-C≡N-^{HS}Fe^{III}-N≡C-W^{IV}-CN-^{HS}Co^{III} and W^V-C≡N-^{HS}Fe^{II}-N≡C-W^V-C≡N-^{HS}Co^{II} states, respectively.

The corresponding **Fe₆Co₃W₆@Mn₉W₆** composite was investigated, where the core crystal (**Fe₆Co₃W₆**) displays a spin transition phase, surrounded by a paramagnetic shell (**Mn₉W₆**). The

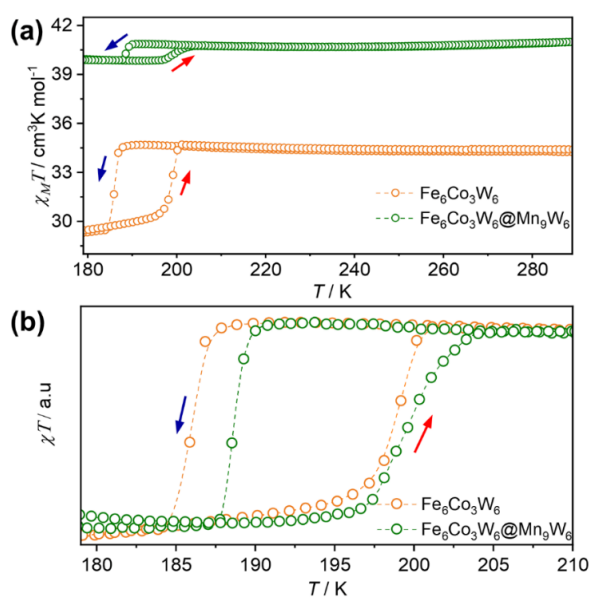


Figure 7. (a) Plots of $\chi_M T(T)$ for seed crystals **Fe₆Co₃W₆** (orange circles) and core-shell crystals **Fe₆Co₃W₆@Mn₉W₆** (green circles) measured upon cooling-heating mode ($H_{dc} = 1000$ Oe, the sweep rate of 1 K/min) (for the detailed description of estimation of $\chi_M T(T)$ for **Fe₆Co₃W₆@Mn₉W₆** see ESI); (b) Normalized data in the transition temperature range.

plots of $\chi_M T(T)$ for **Fe₆Co₃W₆@Mn₉W₆** and for **Fe₆Co₃W₆**, as a reference, are shown in Figure 7. The composite reveals thermal hysteresis of $\chi_M T$ with a critical temperatures $T_{c\downarrow} = 188$ K and $T_{c\uparrow} = 200$ K ($\Delta T = 12$ K), as the clear signature of the core **Fe₆Co₃W₆** phase. A slight increase of the transition temperatures compared to pure **Fe₆Co₃W₆** phase ($T_{c\downarrow} = 186$ K and $T_{c\uparrow} = 199$ K, ($\Delta T =$

13 K) is observed for the composite, which might be explained by considering an ability of the high-spin paramagnetic shell of the largest cell volume (within the whole $\mathbf{M}_9\mathbf{W}_6$ family) to transmit elastic vibrations to the core undergoing SCO. However, as the effect of the shell on the thermal hysteresis is still a complex phenomenon, and other factors such as chemical pressure, shell thickness and crystallites size also play an important role, further magnetic investigations on these mm-sized species should be performed.^{46,47}

The difference in the amplitudes of $\chi_M T(T)$ dependences for $\mathbf{Fe}_6\mathbf{Co}_3\mathbf{W}_6@ \mathbf{Mn}_9\mathbf{W}_6$ composites and for bare $\mathbf{Fe}_6\mathbf{Co}_3\mathbf{W}_6$ crystals at the temperature range of phase transition is represented by the ratio *ca.* 1:4 (Fig. 7). Such proportion illustrates the real average core:shell mass ratio in the measured batch of core-shell crystals, as only the core contributes to the vertical change of the signal in this temperature region. Please, note that the $\chi_M T$ values cannot be derived directly as we do not know the exact masses of each part of composite, and some size polydispersity cannot be avoided, either. This makes our estimations rather semiquantitative, however, the $\chi_M T$ value at room temperature and overall course of the $\chi_M T(T)$ were reasonably reproduced using a simple procedure based on available data for the sole core and sole shell phases (*see* ESI part).

CONCLUSION

In conclusion, we characterized and investigated a new series of 11 binary and even a ternary multicolored core-shell composite molecular crystals, based on isostructural cyanido-bridged polynuclear clusters. For the first time, the magnetic properties of mm sized core-shell crystals, examples of hierarchical crystalline species, undergoing a spin transition, are presented. They were fully characterized from the structural and composition point of views, using XRD and SEM-EDS.

The $\text{Fe}_6\text{Co}_3\text{W}_6@\text{Mn}_9\text{W}_6$ composite exhibits a spin transition and thermal hysteresis, which confirms the coexistence of the thermally switchable core within the high-spin shell, both components being based on isostructural compounds. While notably enriching molecular core-shell domain still being constituted, our studies opens the way for building new mm sized hierarchical architectures based on switchable discrete polymetallic molecules, and thus, introduce a new functional contribution into the fields of molecular magnetism and molecular materials. In the broader context of switchable and magnetic nanoparticle materials shown recently,^{7-10,46,47} our proof-of-concept study may be of value towards new solutions of molecule based switchable systems in micro- and nanoscale.

ASSOCIATED CONTENT

Supporting Information.

The Supporting Information is available free of charge on the ACS Publications website.

Details for structural description, diffraction frames of crystalline composites, face indexing crystal, the data of SEM-EDS and experimental details for magnetic measurements.

Notes

The author declare no competing financial interests.

ACKNOWLEDGMENT

We gratefully acknowledge the financial support from the National Science Center (Poland) research project no. UMO-2019/35/B/ST5/01481 (PI R. Podgajny)

REFERENCES

- 1 Armaroli, N.; Bolink, H. J. *Photoluminescent Materials and Electroluminescent Devices. Topics in Current Chemistry*, Springer, Cham, **2017**
- 2 Hedley, G. J.; Ruseckas, A.; Samuel, I. D. W. Light harvesting for organic photovoltaics. *Chem. Rev.* **2017**, *117*, 796–837.
- 3 Sato, O. Dynamic molecular crystals with switchable physical properties. *Nat. Chem.* **2016**, *8*, 644–656.
- 4 Wang, Y.; Tan, X.; Zhang, Y.-M.; Zhu, S.; Zhang, I.; Yu, B.; Wang, K.; Yang, B.; Li, M.; Zou, B.; Zhang, X.-A. Dynamic behavior of molecular switches in crystal under pressure and its reflection on tactile sensing. *J. Am. Chem. Soc.* **2015**, *137*, 931–939.
- 5 Leong, L. E. K.; Farha, O. K.; Allendorf, M.; Van Duyne, R. P.; Hupp, J. T. Metal-organic framework materials as chemical sensors. *Chem. Rev.* **2012**, *112*, 1105–1125.
- 6 Feng, L.; Wang, K.-Y.; Day, G. S.; Zhou, H.-C. The chemistry of multi-component and hierarchical framework compounds. *Chem. Soc. Rev.* **2019**, *48*, 4823–4853.
- 7 Catala, L.; Brinzei, D.; Prado, Y.; Gloter, A.; Stéphan, O.; Rogez, G.; Mallah, T. Core-multishell magnetic coordination nanoparticles: Toward multifunctionality on the nanoscale. *Angew. Chem. Int. Ed.* **2009**, *48*, 183–187.
- 8 Prado, Y.; Dia, N.; Lisnard, L.; Rogez, G.; Brisset, F.; Catala, L.; Mallah, T. Tuning the magnetic anisotropy in coordination nanoparticles: random distribution versus core-shell architecture. *Chem. Commun.* **2012**, *48*, 11455–11457.

- 9 Risset, O. N.; Quintero, P. A.; Brinzari, T. V.; Andrus, M. J.; Lufaso, M. W.; Meisel, M. W.; Talham, D. R. Light-induced changes in magnetism in a coordination polymer heterostructure, $\text{Rb}_{0.24}\text{Co}[\text{Fe}(\text{CN})_6]_{0.74}@\text{K}_{0.10}\text{Co}[\text{Cr}(\text{CN})_6]_{0.70}\cdot n\text{H}_2\text{O}$ and the role of the shell thickness on the properties of both core and shell. *J. Am. Chem. Soc.* **2014**, *136*, 15660–15669.
- 10 Felts, C.; Slimani, A.; Cain, J. M.; Andrus, M. J.; Ahir, A. R.; Abboud, K. A.; Meisel, M. W.; Boukheddaden, K.; Talham, D. R. Control of the speed of a light-induced spin transition through mesoscale core-shell architecture. *J. Am. Chem. Soc.* **2018**, *140*, 5814–5824
- 11 MacDonald, J. C.; Dorrestein, P. C.; Pilley, M. Foote, M.; M.; Lundburg, M. J. L.; Henning, R. W. A.; Schultz, J.; Manson, J. L. Design of layered crystalline materials using coordination chemistry and hydrogen bonds. *J. Am. Chem. Soc.* **2000**, *122*, 11692–11702
- 12 Ferlay, S.; Hosseini, M. W. Crystalline molecular alloys. *Chem. Commun.* **2004**, 788-789;
- 13 Balogh, C. M.; Veyre, L.; Pilet, G.; Charles, C.; Viriot, L.; Andraud, C.; Thieuleux, C.; Riobé, François F.; Maury, O. Two-color three-state luminescent lanthanide core-shell crystals. *Chem. Eur. J.* **2017**, *23*, 1784–1788.
- 14 Kuzniak, E.; Glosz, D.; Niedzielski, G.; Kobylarczyk, J.; Hooper, M. S.; Hooper, J.; Podgajny, R. Binding of anionic Pt(II) complexes in a dedicated organic matrix: towards new binary crystalline composites. *Dalton. Trans.* **2021**, *50*, 170–185.
- 15 Adolf, C. R. R.; Ferlay, S.; Kyritsakas, N.; Hosseini, M. W. Welding molecular crystals. *J. Am. Chem. Soc.* **2015**, *137*, 15390–15393.
- 16 Paul, M.; Desiraju, G. R. From a binary to a quaternary cocrystal: An unusual supramolecular synthon. *Angew. Chem. Int. Ed.* **2019**, *58*, 12027–12031.

- 17 Catalano, L.; Berthaud, J.; Dushaq, G.; Karothu, D. P.; Rezgui, R.; Rasras, M.; Ferlay, S.; Hosseini, M. W.; Naumov, P. Sequencing and welding of molecular single-crystal optical waveguides. *Adv. Funct. Mater.* **2020**, *30*, 2003443.
- 18 Furukawa, S.; Hirai, K.; Nakagawa, K.; Takashima, Y.; Matsuda, R.; Tsuruoka, T.; Kondo, M.; Haruki, R.; Tanaka, D.; Sakamoto, H.; Shimomura, S.; Sakata, O.; Kitagawa, S. Heterogeneously hybridized porous coordination polymer crystals: Fabrication of heterometallic core-shell single crystals with an in-plane rotational epitaxial relationship. *Angew. Chem. Int. Ed.* **2009**, *48*, 1766–1770
- 19 Wang, L.; Yang, W.; Li, Y.; Xie, Z.; Zhu, W.; Su, Z.-M. Dynamically controlled one-pot synthesis of heterogeneous core-shell MOF single crystals using guest molecules. *Chem. Commun.* **2014**, *50*, 11653–11656.
- 20 Pan, M.; Zhu, Y.-X.; Wu, K.; Chen, L.; Hou, Y.-J.; Yin, S.-Y.; Wang, H.-P.; Fan, Y.-N.; Su, C.-Y. Epitaxial growth of hetero-Ln-MOF hierarchical single crystals for domain- and orientation-controlled multicolor luminescence 3D coding capability. *Angew. Chem. Int. Ed.* **2017**, *56*, 14582–14586.
- 21 Boissonnault, J. A.; Wong-Foy, A. G.; Matzger, A. J. Core-shell structures arise naturally during ligand exchange in metal organic frameworks. *J. Am. Chem. Soc.* **2017**, *139*, 14841–14844.
- 22 Liu, W.; Huang, J.; Yang, Q.; Wang, S.; Sun, X.; Zhang, W.; Liu, J.; Huo, F. Multi-shelled hollow metal-organic frameworks. *Angew. Chem. Int. Ed.* **2017**, *56*, 5512–5516.
- 23 Zhang, F.; Adolf, C. R.; Zigon, N.; Ferlay, S.; Kyritsakas, N.; Hosseini, M. W. Molecular tectonics: hierarchical organization of heterobimetallic coordination networks into heterotrimetallic core-shell crystals. *Chem. Commun.* **2017**, *53*, 3587–3590.

- 24 Yang, X.; Yuan, S.; Zou, L.; Drake, H.; Zhang, Y.; Qin, J.; Alsalmeh, A.; Zhou, H.-C. One-step synthesis of hybrid core-shell metal-organic frameworks. *Angew. Chem. Int. Ed.* **2018**, *57*, 3927–3932.
- 25 Abdallah, A.; Daiguebonne, C.; Suffren, Y.; Rojo, A.; Demange, V.; Bernot, K.; Calvez, G.; Guillou, O. Microcrystalline core-shell lanthanide-based coordination polymers for unprecedented luminescent properties. *Inorg. Chem.* **2019**, *58*, 1317–1329.
- 26 Zhang, X.; Zhu, T.; Ji, C.; Yao, Y.; Luo, J. In situ epitaxial growth of centimeter-sized lead-free (BA)₂CsAgBiBr₇/Cs₂AgBiBr₆ heterocrystals for self-driven X-ray detection. *J. Am. Chem. Soc.* **2021**, *143*, 20802–20810.
- 27 Zhong, Z.-J.; Seino, H.; Mizobe, Y.; Hidai, M.; Fujishima, A.; Ohkoshi S.; Hashimoto, K. A high-spin cyanide-bridged Mn₉W₆ cluster ($S = 39/2$) with a full-capped cubane structure. *J. Am. Chem. Soc.* **2000**, *122*, 2952–2953.
- 28 Bonadio, F.; Gross, M.; Stoeckli, H.; Decurtins, S. High-spin molecules: synthesis, X-ray characterization, and magnetic behavior of two new cyano-bridged Ni^{II}₉Mo^V₆ and Ni^{II}₉W^V₆ clusters with a $S = 12$ ground state. *Inorg. Chem.* **2002**, *41*, 5891–5896.
- 29 Song, Y.; Zhang, P.; Ren, X.-M.; Shen, X.-F.; Li, Y.-Z.; You, X.-Z. Octacyanometallate-based single-molecule magnets: Co^{II}₉M^V₆ (M = W, Mo). *J. Am. Chem. Soc.* **2005**, *127*, 3708–3709.
- 30 Chorazy, S.; Podgajny, R.; Nogaś, W.; Nitek, W.; Kozieł, M.; Rams, M.; Juszyńska, E.; Żukrowski, J.; Kapusta, C.; Nakabayashi, K.; Fujimoto, T.; Ohkoshi, S.; Sieklucka, B. Charge transfer phase transition with reversed thermal hysteresis loop in the mixed-valence Fe₉[W(CN)₈]₆ xMeOH cluster. *Chem. Commun.* **2014**, *50*, 3484–3487.
- 31 Larionova, J.; Gross, M.; Pilkington, M.; Andres, H.; Stoeckli-Evans, H.; Güdel, H. U.; Decurtins, S. High-spin molecules: a novel cyano-bridged Mn₉^{II}Mo₆^V molecular cluster with

- a $S = 5/2$ ground state and ferromagnetic intercluster ordering at low temperatures. *Angew. Chem. Int. Ed.* **2000**, *39*, 1605–1609.
- 32 Ruiz, E.; Rajaraman, G.; Alvarez, S.; Gillon, B.; Stride, J.; Clérac, R.; Larionova, J.; Decurtins, S. Symmetry and topology determine the $\text{Mo}^{\text{V}}\text{-CN-Mn}^{\text{II}}$ exchange interactions in high-spin molecules. *Angew. Chem. Int. Ed.* **2005**, *44*, 2711–2715.
- 33 Podgajny, R.; Chorazy, S.; Nitek, W.; Rams, M.; Majcher, A. M.; Marszałek, B.; Żukrowski, J.; Kapusta, C.; Sieklucka, B. Co-NC-W and Fe-NC-W electron-transfer channels for thermal bistability in trimetallic $\{\text{Fe}_6\text{Co}_3[\text{W}(\text{CN})_8]_6\}$ cyanido-bridged cluster. *Angew. Chem. Int. Ed.* **2013**, *52*, 896–900.
- 34 Chorazy, S.; Stanek, J. J.; Nogaś, W.; Majcher, A. M.; Rams, M.; Kozieł, M.; Juszyńska, E.; Nakabayashi, K.; Ohkoshi, S.; Sieklucka, B.; Podgajny, R. Tuning of charge transfer assisted phase transition and slow magnetic relaxation functionalities in $\{\text{Fe}_{9-x}\text{Co}_x[\text{W}(\text{CN})_8]_6\}$ ($x = 0-9$) molecular solid solution. *J. Am. Chem. Soc.* **2016**, *138*, 1635–1646.
- 35 Kobylarczyk, J.; Liberka, M.; Stanek, J. J.; Sieklucka, B.; Podgajny, R. Tuning of the phase transition between site selective SCO and intermetallic ET in trimetallic magnetic cyanido-bridged clusters. *Dalton Trans.* **2020**, *49*, 17321–17330.
- 36 Chorazy, S.; Majcher, A. M.; Kozieł, M.; Kobylarczyk, J.; Ohkoshi, S.; Podgajny, R. Tuning of High spin ground state and slow magnetic relaxation within trimetallic cyanide-bridged $\{\text{Ni}^{\text{II}}_x\text{Co}^{\text{II}}_{9-x}[\text{W}(\text{CN})_8]_6\}$ and $\{\text{Mn}^{\text{II}}_x\text{Co}^{\text{II}}_{9-x}[\text{W}(\text{CN})_8]_6\}$ clusters. *Chem. Eur. J.* **2018**, *24*, 15533–15542.
- 37 Szklarzewicz, J.; Matoga, D.; Lewiński, K. $\text{K}_4[\text{Mo}(\text{CN})_8]$ solution: X-ray crystal structure of $(\text{PPh}_4)_2[\text{Mo}(\text{CN})_4\text{O}(\text{NH}_3)] \cdot 2\text{H}_2\text{O}$. *Inorg. Chim. Acta.* **2007**, *360*, 2002–2008.

- 38 Pribush, R.; Archer, R. D. Transition metal eight-coordination. VI. Isomerization through electronic and environmental effects—electron spin resonance, magnetic circular dichroism, and electronic spectra of Octacyanotungstate(IV) and (V). *Inorg. Chem.* **1974**, *13*, 2556–2563.
- 39 SAINT Software Users Guide, Version 7.0; Bruker Analytical X-Ray Systems: Madison, WI, **1999**.
- 40 Sheldrick, G. M. SADABS, Version 2.03; Bruker Analytical X-Ray Systems, Madison, WI, **2000**.
- 41 Macrae, C. F.; Edgington, P. R.; McCabe, P.; Pidcock, E.; Shields, G. P.; Taylor, R.; Towler, M.; Streek, J. Mercury: visualization and analysis of crystal structures. *J. Appl. Crystallogr.* **2006**, *39*, 343–350
- 42 Bain, G. A.; Berry, J. F. Diamagnetic corrections and Pascal's constants. *J. Chem. Educ.* **2008**, *85*, 532–536.
- 43 Luo, T. M.; MacDonald, J. C.; Palmore, G. T. R. Fabrication of complex crystals using kinetic control, chemical additives, and epitaxial growth. *Chem. Mater.* **2004**, *16*, 4916–4927.
- 44 Brès, E. F.; Ferlay, S.; Dechambenoit, P.; Leroux, H.; Hosseini, M. W.; Reyntjens, S. Investigations on crystalline interface within a molecular composite crystal by microscopic techniques. *J. Mater. Chem.* **2007**, *17*, 1559–1562.
- 45 Raza, Y.; Volatron, F.; Moldovan, S.; Ersen, O.; Huc, V.; Martini, C.; Brisset, F.; Gloter, A.; Stéphan, O.; Bousseksou, A.; Catala, L.; Mallah, T. Matrix-dependent cooperativity in spin crossover Fe(pyrazine)Pt(CN)₄ nanoparticles. *Chem. Commun.* **2011**, *47*, 11501–11503.
- 46 Wang, Y.-X.; Qiu, D.; Xi, S.-F.; Ding, Z.-D.; Li, Z.; Li, Y.; Ren, X.; Gu, Z.-G. Iron(II)-triazole core-shell nanocomposites: toward multistep spin crossover materials. *Chem. Commun.* **2016**, *52*, 8034–8037.

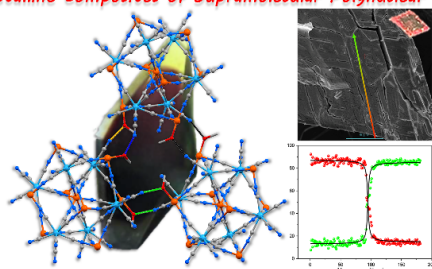
- 47 Slimani, A.; Khemakhem, H.; Boukhedden, K. Structural synergy in a core-shell spin crossover nanoparticle investigated by an electroelastic model. *Phys. Rev. B.* **2017**, *95*, 174104.
- 48 Felix, G.; Nicolazzi, W.; Salmon, L.; Molnár, G.; Perrier, M.; Maurin, G.; Larionova, J.; Long, J.; Guari, Y.; Bousseksou, A. Enhanced cooperative interactions at the nanoscale in spin crossover materials with a first-order phase transition. *Phys. Rev. Lett.* **2013**, *110*, 235701.
- 49 Quintero, C. M.; Félix, G.; Suleimanov, I.; Sánchez Costa, J.; Molnár, G.; Salmon, L.; Nicolazzi, W.; Bousseksou, A. Hybrid spin-crossover nanostructures. *Beilstein J. Nanotechnol.* **2014**, *5*, 2230–2239.

For Table of Contents Use Only

Binary and Ternary Core-Shell Crystals of Polynuclear Coordination Clusters via Epitaxial Growth

Le Shi, Jędrzej Kobylarczyk, Kamil Kwiatkowski, Barbara Sieklucka, Sylvie Ferlay, and Robert Podgajny*

Crystalline Composites of Supramolecular Polynuclear Clusters



The colourful mm sized core-shell crystals were designed and prepared from functional magnetic polynuclear clusters phases, using the epitaxial growth method. The switchable ET/CTIST core was successfully enveloped in paramagnetic shell to reveal the thermal hysteresis loop.